Soft Matter

Sodium dodecyl sulfate modulates the structure and rheological properties of Pluronic F108 - poly(acrylic acid) coacervates

Journal:	*Soft Matter*
Manuscript ID	SM-ART-09-2021-001273.R2
Article Type:	Paper
Date Submitted by the Author:	30-Nov-2021
Complete List of Authors:	Gong, Ziyuan; University of Akron, Polymer Engineering Zacharia, Nicole; University of Akron, Polymer Engineering Vogt, Bryan; Penn State - Main Campus, Chemical Engineering

ARTICLE

Sodium dodecyl sulfate modulates the structure and rheological properties of Pluronic F108 - poly(acrylic acid) coacervates

Received 00th January 20xx,
Accepted 00th January 20xx

DOI: 10.1039/x0xx00000x

Ziyuan Gong,[a,†] Nicole S. Zacharia, [a,*] and Bryan D. Vogt[b,*]

Micelles formed within coacervates phases can impart functional properties, but it is unclear if this micellization provides mechanical reinforcement of the coacervate whereby the micelles act as high functionality crosslinkers. Here, we examine how sodium dodecyl sulfate (SDS) influences the structure and properties of Pluronic F108-polyacrylic acid (PAA) coacervates as SDS is known to decrease the aggregation number of Pluronic micelles. Increasing the SDS concentration leads to larger water content in the coacervate and an increase in the relative concentration of PAA to the other solids. Rheological characterization with small angle oscillatory shear (SAOS) demonstrates that these coacervates are viscoelastic liquids with the moduli decreasing with the addition of the SDS. The loss factor (tan δ) initially increases linearly with the addition of SDS, but a step function increase in the loss factor occurs near the CMC of SDS. However, this change does not appear to be correlated with any large scale structural differences in the coacervate as determined by small angle x-ray scattering (SAXS) with no signature of Pluronic micelles in the coacervate when SDS concentration is > 4 mM during formation of the coacervate, which is less than observed (6 mM SDS) in initial Pluronic F108 solution despite the higher polymer concentration in the coacervate. These results suggest that the mechanical properties of polyelectrolyte-non-ionic surfactant coacervates are driven by the efficicacy of binding between the complexing species driving the coacervate, which can be disrupted by competitive binding of the SDS to the Pluronic.

1. Introduction

The entropy associated with the counterions on polyelectrolytes (PEs) tends to provide the driving force for phase separation of mixtures of polyanions and polycations through the formation of polyelectrolyte complexes (PECs),[1-3] but enthalpic effects can be significant with PECs formed from weak polyelectrolytes.[4] These PECs can be separated into two general classes: coacervates,[5, 6] where both phases are liquids (liquid-liquid phase separation), and solid complexes, where the complex precipitates from the aqueous phase (liquid-solid phase separation).[7] The phase behaviour for these PECs are not only functions of temperature[8] and stoichiometry,[9] but also pH[10] and salts present.[11] These factors can be used to manipulate the complexation process by mediating[12] or exasperating[13] the interactions responsible for formation of the PECs. The coacervate phase is of particular interest for a variety of applications due to its aqueous liquid-like environment and tuneable rheological properties.[14] For example, coacervates alter the rheology of food product to improve the efficiency of processing while providing the desired product texture.[15] Moreover, unlike most other biphasic systems involving water, surface tension between phases is not large for coacervates.[16] The lack of surface tension for coacervates enhances the sequestration of organic molecules from aqueous solution[17] through reduction of transport limitations in comparison to flocculation.[18] Similarly, the coacervate can be used to encapsulate drug or nutraceuticals, such as Omega-3 rich oil,[19] and the lack of surface tension assists with their controlled release *in vitro*. Coacervates also have been demonstrated to be useful for maintaining the particle size of therapeutic nanoparticles,[20] which is critical to drug efficacy.

For drug delivery applications, generation of a coacervate within the core of a micelle[21] provides an environment to promote the drug or protein loading,[22, 23] while the corona can used to alter the response with the environment.[22, 24] The release of cargo within the coacervate micelles can be triggered by salt.[25] Use of triblock copolymers where the end blocks form a coacervate results in a hydrogel[26, 27] that is salt[28] and temperature[29] dependent. These hydrogels are proposed as injectable drug delivery systems, where the viscoelasticity of these hydrogels is key to their utility,[28] but this property is strongly dependent on the morphology.[26] This direct relationship between structure and rheological properties is similar to the relationships developed for other physically crosslinked gels based on van der Waals interactions[30] or hydrophobic interactions[31, 32] as opposed to the coacervate formation. The rheological characterization of simple

[a] Department of Polymer Engineering, University of Akron, Akron, OH 44325.
[b] Department of Chemical Engineering, Pennsylvania State University, University Park, PA 16802
†Present address: Department of Chemistry and Biochemistry, University of South Carolina, Columbia, SC 29208
* To whom correspondence should be addressed: bdv5051@psu.edu (BDV) and nzach1@gmail.com (NSZ)
Electronic Supplementary Information (ESI) available: pH dependent turbidity, ^{1}H NMR spectra, SAOS strain sweeps, coacervate composition, DLS and SAXS profiles of coacervates, SAOS frequency sweeps. See DOI: 10.1039/x0xx00000x

coacervates based on polyanion and polycations has demonstrated that these can be viscoelastic solids[33] or viscoelastic liquids,[34] where addition of salt generally reduces its elastic modulus and viscosity.[35] This reduction in moduli with added salt is consistent with results for the triblock copolymer hydrogels,[28] but the lack of clear structural features in the scattering for these coacervates can challenge the ability to obtain unambiguous structure-property relationships. Previously, a combination of neutron and x-ray scattering was used to probe the chain conformation and concentration fluctuations in coacervates.[36] Schlenoff and co-workers demonstrated that small angle neutron scattering can elucidate the chain conformation from solution to solid PEC.[37] However, this measurement required a specially synthesized perdeuterated polyelectrolyte with a narrow molecular mass distribution.[37]

Self-assembly of surfactants typically leads to well defined structures that can readily be characterized by scattering.[37-39] Alternatively to the coacervation of surfactants as previously described, surfactant-polyelectrolyte complexes have also been extensively examined[40-44] where the hydrophilic head of the surfactant generally interacts with the polyelectrolyte.[45] These complexes can be similar to PECs, but generally are through to be nanostructured due to the self-assembly of the surfactant. Additionally, the hydrophobic domains from the surfactants can assist in sequestering hydrophobic dyes within the coacervate phase of surfactant-polyelectrolyte complexes.[46] The phase behaviour of these surfactant-polyelectrolytes can be altered through composition,[47] molecular mass,[34] salt,[48] and pH[49] similar to PECs. The chain conformation in surfactant-polyelectrolyte coacervates is driven primarily by the persistence length of the polyelectrolyte.[50] Although the rheological properties of surfactant-polyelectrolyte complexes and similar coacervates[51, 52] have been extensively studied,[53-57] there remains a lack of understanding of the nanostructure-rheological property relationships for these materials. By analogy, the mechanical properties of the surfactant containing hydrogels have been demonstrated to be intimately tied to the structure with the surfactants providing effective crosslinks,[58] so it is expected that the surfactant structure within the complex would control its mechanical response.

For surfactant-polyelectrolyte complexes, the addition of a second surfactant can act to promote precipitation[59] or miscibility of the components.[60] Similar effects have been demonstrated for hydrophobically crosslinked hydrogels where sodium dodecyl sulfate (SDS) leads to enhanced mechanical strength at low concentrations, but additional solvation of the supramolecular bonds by the SDS can cause the hydrogel to dissolve.[61] The phase behaviour of surfactant-polyelectrolyte complexes are dependent on the mixed micelle composition to provide an opportunity for tuning coacervates.[44, 62-64] The use of mixed micelles also provides the opportunity to manipulate the structure of the micelle to enable examination into how the micelle structure influences the mechanical properties of coacervates. One of the most commonly examined systems is Pluronic-SDS, where the addition of SDS tends to suppress the formation of micelle.[65, 66] This change in micellization behaviour was initially attributed to the binding of SDS with the hydrophobic centre block of the Pluronic copolymer,[67, 68] but subsequent some investigations demonstrated that binding of SDS to the ethylene oxide (EO) repeat units in Pluronic, [69] likely through interactions between the sulfate group and the ether oxygen. The behaviour of the SDS-Pluronic interactions is rich with micelles of SDS able to bind to single Pluronic chains.[70] Similarly, SDS molecules below the CMC bind to Pluronic micelles and individual chains.[71] Complex formation between SDS and PEO alone has been predicted from a theoretical molecular thermodynamics framework as well,[72] so there is clear evidence for the binding of SDS with PEO. However from recent SANS measurements and comparisons of the binding of PPO and PEO with SDS, there is evidence that the binding of SDS is stronger for the PPO than PEO.[69]

We have previously reported that the coacervate structure is altered when poly(ethylene glycol) is replaced by Pluronic surfactants in coacervates with poly(acrylic acid) (PAA)[46] where small angle x-ray scattering (SAXS) indicates the micelles of Pluronic persist in the coacervate. However, the effective phase diagram for these two coacervates is not significantly altered between the complexation of the Pluronic micelles or the PEG chains with PAA with the differences potentially due to the small differences in the molecular masses.[46] This suggests that the underlying physics governing the complexation associated with coacervation is not significantly altered by the amphiphilic nature of the Pluronic in this case. Here we report on the manipulation of this nanostructure with mixed micelles consisting of SDS and Pluronic. The structure and rheological properties of coacervates of PAA -Pluronic F108 are impacted by the inclusion of SDS as a cosurfactant, which modulates micellization as well as the composition of the coacervate. The addition of SDS in the surfactant-polyelectrolyte coacervates led to increased water content and PAA concentration, while the Pluronic concentration decreases. These changes decreased the elastic moduli of the coacervates from small angle oscillatory shear (SAOS) measurements. A large increase in tan δ of the coacervates occurred near the critical micelle concentration (CMC) for neat SDS,[73] which may be associated with a change in the binding between the EO segments and SDS as has been theoretically shown. [72] However, the SAXS patterns for the coacervates are not significantly altered just above and below the CMC of SDS, which would indicate this change to be more compositional in nature than structural. The influence of SDS on micellization within the coacervate is more pronounced than we previously demonstrated with more well defined mixed micelles.[67] Here, the viscoelastic properties of the coacervate do not appear correlated with the micelle structure. The water content increases with increasing SDS concentration, but the water content can be similarly altered by changing the pH during coacervation without SDS, while maintaining the micellization of the Pluronic, which leads to nearly invariant viscoelastic properties irrespective of water content. Instead, we attribute the mechanical changes to be driven almost

entirely by the Pluronic concentration that decreases with increasing SDS concentration. As the network of the coacervate is driven by the complexation between PAA and the EO segments of the Pluronic, the loss of Pluronic will lead to an effectively lower crosslink density for the associated network. These results suggest that the SDS interacts with the EO segments to reduce the ability for tight complexation of multiple segments on a single chain due to the presence of the hydrophobic alkyl tail of adsorbed SDS .

2. Experimental methods

2.1 Materials

Poly(acrylic acid) (PAA, 25 wt% aq., nominal M_W = 50,000 g/mol) was purchased from Polysciences, Inc. Pluronic F108 (F108 pastille, $PEO_{132}PPO_{50}PEO_{132}$, nominal M_W=14,600 g/mol) was obtained from BASF. Deuterated dimethyl sulfoxide (DMSO-d6, 99.9% atom D) was purchased from Cambridge Isotope Laboratories Inc. Sodium dodecyl sulfate (SDS, ACS reagent, ⩾ 99%) was purchased from Sigma-Aldrich. Deionized water (DI-water) was purified by a Milli-Q DQ-3 system (Millipore, Bedford, MA, USA) to a resistivity of 18.2$M\Omega$.

2.2 Coacervate preparation

The coacervates were prepared by mixing aqueous solutions of F108/SDS and PAA as illustrated pictorially in Figure 1. The surfactant solution contained 105 mM F108 relative to the PEO repeat with the SDS in this solution, $[SDS]_{Sol}$, systematically varied from 0-20 mM. The PAA solution was prepared at $[PAA]_{Sol}$ = 40 mM (relative to the monomer repeat unit) in water. Equal volumes of these two solutions (PAA and F108/SDS) were combined and stirred for 1 h at 25 ºC. This initial mixing produced a transparent, single phase solution. The pH was subsequently adjusted to pH=2.0 by dropwise addition of dilute HCl (1 M). The selection of pH=2.0 for the coacervate fabrication was based on turbidimetric titrations of the SDS-free solution (Figure S1). The PAA is fully protonated at this pH to promote hydrogen bonding with the ether oxygen in the F108, which induced liquid-liquid phase separation (coacervation) as shown in Figure 1. 30 min after the pH adjustment, the polymer-rich coacervate phase was collected by centrifugation at 9000 rpm for 30 min. As control experiments, coacervates containing only F108 and PAA were fabricated using the same methods but at different pH (pH = 2.0, 2.3, 2.7, 3.0). This systematically alters the water content of the coacervate while maintaining the micelle structure of the F108 within the coacervate.

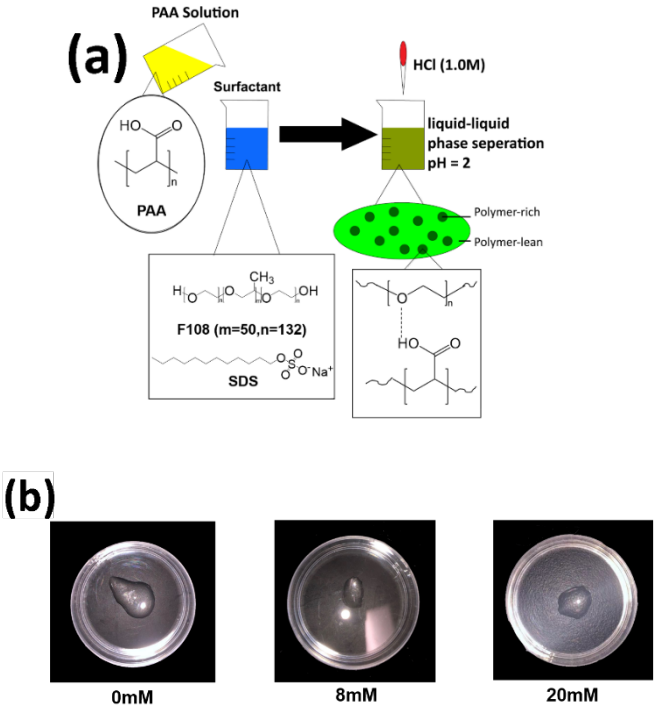

Fig.1 (a) Schematic illustrating the process to prepare the PAA/F108/SDS coacervates. The concentration of F108 and PAA in the solutions was held constant with the SDS concentration systematically varied from 0 to 20 mM. **(b)** Images of the coacervates with different SDS content.

2.3 Composition of the coacervate

To determine the water content of the coacervate phase, a known amount of the collected coacervate was dried under vacuum for at least 24 h at 50 ºC and determined to be fully dried when there was less than 5% mass change after an additional 2 h. From NMR of the dried coacervates, there is minimal water remaining under these drying conditions. The mass difference associated with the as-collected and dried coacervate was used to estimate the water content (w_{H2O}) as:

$$w_{H_2O} = \frac{m_w - m_d}{m_w} \times 100\% \qquad (1)$$

where m_w is the mass of the as collected (wet) coacervate and m_d is the mass of the coacervate after drying. Each coacervate was fabricated at least 3 times to determine the average water content.

Solution state ^{1}H NMR spectroscopy (Varian MERCURY 300 MHz spectrometer) was used to determine the composition of the solid components (F108, PAA, SDS) in the coacervate. Approximately 7 mg of dried coacervate was dissolved in 7 mL DMSO-d6 for the measurements. Control spectra of the PAA, F108, SDS were also obtained in DMSO-d6. Figure S2 illustrates the NMR spectra for the individual components and the coacervate prepared with $[SDS]_{Sol}$ = 20 mM. The peak assignments associated with the different components are shown in Table S1. The overlapping peaks of the PAA and SDS challenge the direct determination of the coacervate composition, so a deconvolution procedure was used to

calculating the composition from NMR as described in the Electronic Supplementary Information (ESI). To test this deconvolution procedure, the composition from ^{1}H NMR on a known mixture of PAA, F108 and SDS was found to be in good agreement as shown in Figure S3.

2.4 Rheological characterization

To examine the influence of the addition of SDS to the PAA/F108 coacervate on their rheological properties, small amplitude oscillation shear (SAOS) was performed using Advanced Rheometric Expansion System (ARES-G2, TA Instruments) rheometer, which was equipped with 8 mm upper plate and 25 mm lower plate with a solvent trap. The supernatant (polymer poor phase) was transferred from the centrifuge tube to the solvent trap to prevent dehydration of the coacervate during testing, while not altering the composition of the coacervate as these phases are in equilibrium. A strain sweep experiment from 0.1% to 200% at 1 rad/s was used to determine the linear viscoelastic (LVE) region (Figure S4). For all compositions, 3 % strain was within the LVE regime and used for frequency sweeps from 0.1 rad/s to 100 rad/s to determine the frequency dependent storage modulus (G'), loss modulus (G") and loss factor (tan δ) at 25 ºC.

2.5 Structural characterization

The size of the F108 micelles as a function of SDS concentration in solution was determined from dynamic light scattering (DLS, ZetaPALS Potential Analyzer, Brookhaven Instrument). Aqueous solutions were prepared at 0.5 wt% F108 with $0 \leq [SDS]_{Sol} \leq 20$ mM. All solutions were filtered (0.45 µm, Nylon, Millipore) prior to measurements. The DLS measurements were performed at 25 ºC $\pm$ 0.2 ºC with the time dependent scattered intensity measured at 90º. Each composition was measured in triplicate. The autocorrelation function was fit to the CONTIN model to obtain the average hydrodynamic diameter, polydispersity and average diffusion coefficient.

The nanostructure of the coacervates was characterized by small angle x-ray scattering (SAXS) performed on the Complex Materials Scattering (CMS, 11-BM) at the National Synchrotron Light Source II (NSLS-II, Brookhaven National Laboratory, New York, U.S.A). The coacervate was sealed in Boron-rich capillary tubes (Charlessupper Co.) with a wall thickness of 10 µm and outer diameter of 1 mm. The SAXS measurements used an X-ray wavelength (λ) of 0.918Å and the sample-to-detector distance was 5 m. The scattering was measured over a momentum transfer vector (q) range between 0.01 Å^{-1} and 0.13 Å^{-1}using a pixel-array detector (Dectris Pilatus 2M, pixel size = 0.172 mm x 0.172 mm). A silver behenate standard was used to calibrate the q range. The 2D scattering data were corrected for the background using an empty capillary and then azimuthally averaged to obtain 1D scattering profiles.

These 1D SAXS profiles were fit to the correlation length model developed by Hammouda[74] that has been shown to describe the scattering of polymer solutions with associations and covalently crosslinked hydrogels.[75, 76] This model uses a power law to describe fluctuations at length scales greater than the measured q range and a Lorentzian function to describe the scattering from chains in solution as:

$$I(q) = \frac{A}{q^n} + \frac{C}{1+(q\xi_L)^m} + B \qquad (2)$$

where A and C are scale terms that includes contrast and the other prefactors, n is a Porod exponent that describes the fractal dimensions of the large size heterogeneities, ξ_L is a correlation length associated with the chains that describes the mesh size of the physical network of the coacervates, m is the Lorentzian exponent that typically depends on the polymer-solvent interactions, and B is the background. However, the structure of this model cannot describe well defined correlations, such as those expected from the self-assembly of the amphiphiles. To describe the scattering where micelles persist in the coacervate, a Lorentzian term was added to eqn (2) that the describes these correlations.

$$I(q) = \frac{A}{q^n} + \frac{C}{1+(q\xi_L)^m} + \frac{D}{(q-q_0)^2+\delta} + B \qquad (3)$$

where D is a scaling term, q_0 is the size of the assembled structure in Fourier space and δ is associated with the width of the peak. This term was only included in the fit when required to improve the fit quality. At $[SDS]_{sol}$ =1.5 mM, the fit quality is slightly improved with the added term, but this leads to issues in convoluting the effects of the 2nd and 3rd terms in eqn(3) to provide values that are limited in their sensitivity (Table S2 provides the relevant fit parameters).

3. Result and discussion

Coacervates containing PAA, F108, and SDS were fabricated at pH = 2 as illustrated pictorially in Figure 1a. Mixing PAA and F108 aqueous solutions at sufficiently low pH (Figure S1) leads to liquid-liquid phase separation whereby a polymer rich coacervate phase is formed. Mixtures of SDS and PAA yield a single aqueous phase (Figure S5). The addition of SDS to the coacervate of PAA and F108 does not appreciable change its appearance as shown in Figure 1b. Although there is limited visual change, the coacervate flows more readily at the highest concentrations of SDS, which demonstrates some change in the rheological properties. As it is known that the size of Pluronic micelles is reduced with addition of SDS,[77] these changes in structure may be related with the observed differences in the flow properties of the coacervates.

3.1 Influence of SDS on the coacervate composition

The composition of the solids in the coacervate (PAA, F108 and SDS) was determined using ^{1}H NMR as described in the ESI. Figure 2 illustrates how the composition of the coacervate is related to the concentration of SDS in the initial solution. Without SDS, the coacervate contains more F108 than PAA. As the SDS concentration in the solution increases, there is a continual decrease in the F108 concentration in the coacervate. The fraction of PAA in the coacervate is invariant when $[SDS]_{sol}$

is less than 3 mM, but then increases with increasing SDS at higher concentrations. The coacervate becomes PAA rich at $[SDS]_{sol}$ = 4 mM. The SDS concentration in the coacervate remains below 5 wt% irrespective of $[SDS]_{sol}$. The SDS content is statistically constant for $[SDS]_{sol}$ > 2 mM. This result suggests that the SDS changes the nature of the interaction between F108 and PAA.

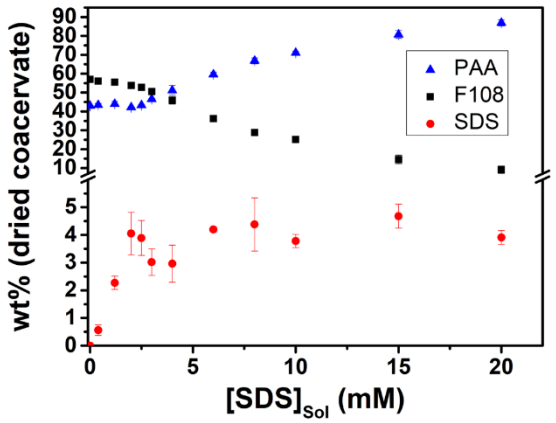

Fig. 2. Composition of the solid components, (▲) PAA, (■) F108, and (●) SDS, in the coacervate as determined from ^{1}H NMR. These values exclude the water content in the coacervate.

The inclusion of SDS does alter the ion content in the solution as it is a charged surfactant. As shown in Figure 3, the water content in the coacervate increases monotonically as $[SDS]_{sol}$ increases. Schlenoff and coworkers[12] have reported a similar phenomenon for PSS/PDADMA coacervates where increasing salt concentration will lead to higher water content in the coacervate, although the salt is generally mostly excluded from the polymer rich coacervate phase.[78] The coupling of salt and concentration effects can challenge the interpretation of the effect of salts on rheological properties.[79] It is known that SDS interacts with the PPO segments of Pluronic F108,[67] but SDS can also interact with the EO segments via sulfate-ether oxygen. [69] The addition of the SDS would in general act to increase the hydrophilicity of the coacervate. As PAA and the head of SDS surfactant are both negatively charged, these should not be interacting favorably. Thus, the increase in the PAA and SDS as a fraction of the solid phase simultaneously in the coacervate is unexpected.

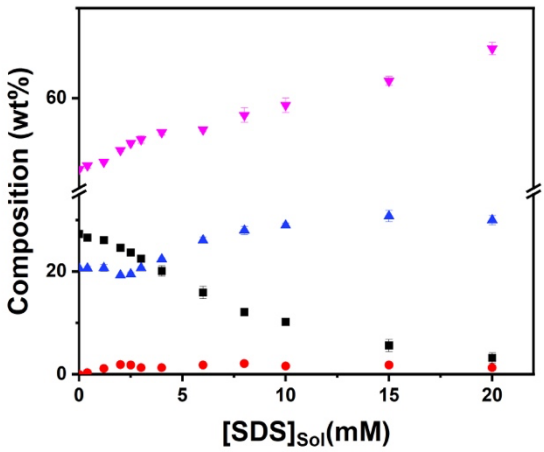

Fig. 3. Overall composition of the coacervates (▲) PAA, (■) F108, (●) SDS, and (▼) water as a function of the SDS concentration in the initial solution used in the fabrication of the coacervates.

The near linear increase in water content with the concentration of SDS in solution is surprising as the content of SDS in the solid coacervate is essentially invariant for $[SDS]_{sol}$ > 2 mM (Figure 2), while there is an approximately 15 % increase in the amount of water for 2 mM < $[SDS]_{sol}$ < 20 mM. If we normalize for the change in water content, the composition of the coacervate can provide more insights as shown in Figure 3 and Table 1. The overall concentration of the PAA in the coacervate still increases at high $[SDS]_{sol}$, despite the significant increase in the water content. The normalized composition of the coacervate is shown in Figure 3. The decrease in the F108 concentration in the coacervate is significant at high $[SDS]_{sol}$ going from approximately 25 wt % of the coacervate to less than 5 % when $[SDS]_{sol}$ = 20 mM. As the coacervate forms from the hydrogen bonding between the EO segment in F108 and the PAA, the large reduction in the concentration of F108 will decrease the number of hydrogen bonds that hold the coacervate and this will produce a looser effective network in the coacervate. By analogy to physically crosslinked hydrogels,[32] this change in network structure would be expected to increase the swelling, consistent with the increased water content observed for these coacervates. These results indicate that the SDS impacts the ability for the EO segments in the Pluronic to bind with the PAA. From a simple strength of the interaction, a single sulfate-ether oxygen (SDS-EO) interaction should be more favourable energetically than the carboxylic acid-ether oxygen (AA-EO) interaction, but the high concentration of PAA should allow for some replacement of SDS-EO with AA-EO especially below the CMC.[80] However, the initial complex formed tends to control the coacervate concentration as diffusion within the concentrated coacervate phase is difficult. Nonetheless, decreasing EO binding sites available by the SDS would generally lead to expectations that the PAA concentration should decrease. Thus, additional insights from the structure and properties of these coacervates is necessary

to understand how SDS induces these compositional changes to the coacervates.

Table 1. Overall composition of PAA/F108/SDS coacervate estimated from ^{1}H NMR and the water content from drying.

$[SDS]_{Sol}$ (mM)	Coacervate composition (wt%)			w_{H2O} (wt%)
	PAA	F108	SDS	
0	20.6±0.1	27.3±0.1	0.00	52.1±0.2
0.5	20.6±0.4	26.6±0.5	0.3±0.1	52.5±0.3
1.5	20.7±0.7	26.1±0.3	1.1±0.1	52.9±0.1
2	19.3±0.1	24.6±0.5	1.9±0.4	54.2±0.2
2.5	19.5±0.3	23.7±0.3	1.8±0.3	55.0±0.1
3	20.7±0.2	22.5±0.1	1.3±0.5	55.4±0.4
4	22.4±0.2	20.1±1.0	1.3±0.4	56.2±0.3
6	26.1±0.6	15.9±1.2	1.8±0.1	56.5±0.2
8	28.0±0.8	12.1±0.3	2.1±0.5	58.1±0.8
10	29.0±0.4	10.2±0.3	1.6±0.1	59.2±0.8
15	30.8±1.1	5.6±1.2	1.8±0.2	61.9±0.5
20	30.0±0.9	3.2±1.0	1.3±0.2	65.5±0.7

3.2 Impact of SDS on the structure of coacervates

This large change in the composition of the coacervate would be expected to lead to large changes in its structure. To put the changes in structure of the coacervate in context, the structure of the Pluronic F108 micelles with added SDS were first examined using DLS (Figure S6). Figure 4 illustrates how the micelle size changes with the addition of SDS. It should be noted that the concentration used for these DLS studies is less than the CMC reported in earlier papers for Pluronic F108,[81] but similar to some more recent reports for the CMC of F108.[82] This difference may be due to some changes in the composition of this polymer from batch to batch variation. Without SDS, the hydrodynamic diameter is consistent with expectations for a micelle of Pluronic F108.[81] The addition of SDS initially decreases the hydrodynamic diameter with a minimum size at $[SDS]_{sol}$ = 10 mM. This minimum size is similar to that of unimers in solution when the concentration of Pluronic is below its CMC. This decrease in the size of the Pluronic F108 micelle from the addition of SDS is consistent with prior reports for Pluronic-SDS in general.[65, 67] At higher $[SDS]_{sol}$, there is a small increase in the hydrodynamic diameter (Figure 4). We attribute this increase in hydrodynamic diameter to the formation of SDS micelles that can add to the F108 as well as the CMC of SDS is 8.2 mM.[73] The adsorption of SDS on the F108 decreases the free solution concentration of SDS, but both SDS unimers and micelles can interact with Pluronic.[69] These results suggest that the F108 micelles appear to persist to at least 6 mM of SDS from the hydrodynamic diameter. The size of Pluronic-SDS aggregates at $[SDS]_{sol}$= 8 is near the unimer size and thus unlikely to be a mixed micelle. The micelle size (aggregation number of the Pluronic) decreases due to the interaction between the SDS and the F108, which produces mixed micelles.[67] Thus, it is expected that the coacervates will not contain micelles when $[SDS]_{sol}$ >6- 8 mM.

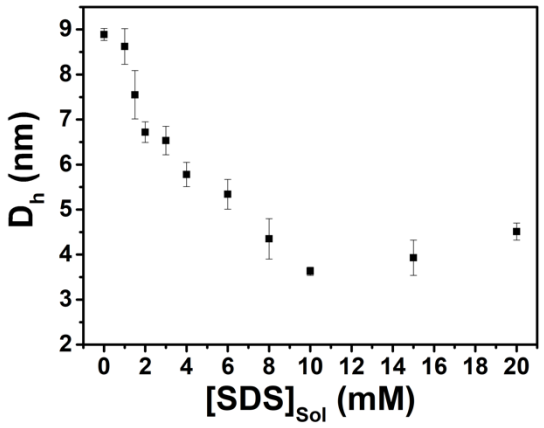

Fig. 4. Hydrodynamic diameter of F108 micelle as a function of $[SDS]_{Sol}$ in solution. The concentration of F108 is held constant at 0.5 wt% (89.25 mM).

Figure 5 illustrates the SAXS patterns associated with structure of the coacervates as a function of SDS concentration used in the preparation of the coacervate. Individual SAXS patterns for all of the $[SDS]_{sol}$ examined are shown in Figure S7. Without SDS, the scattering profile contains a well-defined peak centred at approximately 0.047 Å^{-1}, which corresponds to a size of approximately 13.3 nm. This is similar to the hydrodynamic radius of the F108 micelle, so we can tentatively attribute this correlation peak to the micelles incorporated in the coacervate. Additionally, there is an increase in scattered intensity at low *q*, which is associated with larger scale heterogeneities in the coacervate. The addition of $[SDS]_{sol}$ = 1 mM leads to limited change in the low *q* scattering, but the peak associated with the micelles shifts to lower *q* and broadens significantly. This change is consistent with the expectation for decreased micelle size with the introduction of SDS, but the broadening of the peak is indicative that a broad distribution of sizes is present within the coacervate. At higher concentrations, the peak evolves to a shoulder and no features associated with the micelles are observable at $[SDS]_{sol}$ = 10 mM. To better quantify the structure from the SAXS measurements, the profiles were fit to a correlation length model that includes an additional correlation term to describe well defined self-assembled structures.

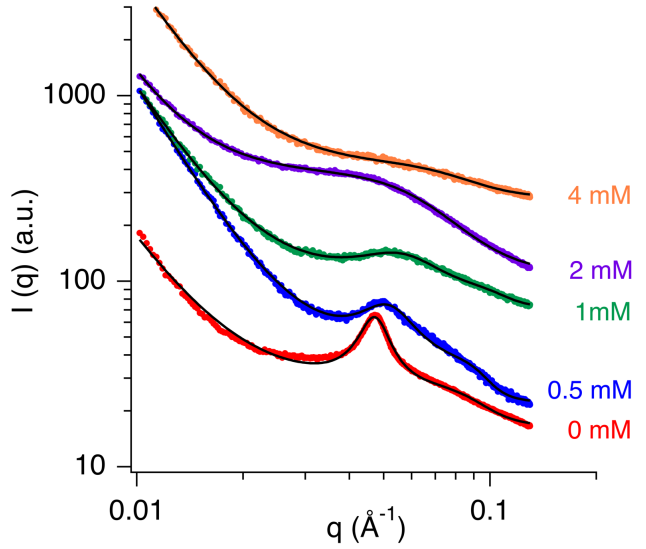

Fig. 5 Impact of $[SDS]_{sol}$ on the SAXS profiles of the coacervates. The black solid line is the fit of the data. The scattering profiles for the different SDS concentrations have been shifted vertically for clarity.

The scattering data can be well represented by these models. The key parameters obtained from the fits of the SAXS data are listed in Table S2. From these model, two primary structural characteristics are obtained associated with all of the coacervates: a characteristic exponent associated with the large scale fluctuations that give arise to the low *q* upturn in the scattering and the characteristic length of the polymers in the coacervate. Additionally, the size of micelles assembled within the coacervates is obtained at low $[SDS]_{sol}$. The effect of $[SDS]_{Sol}$ on the large length scale fluctuations in the system, the apparent mesh size for the physical network from the coacervate and the micelle structure in the coacervate is quantified in Figure 6. As shown in Figure 6a, the Porod exponent associated with the increased scattering at low *q* is essentially independent of the SDS concentration used in the formation of the coacervate. This exponent being near 3 is indicative of a clustered network for the scatterers as expected for the network structure of the coacervates. The length scales for these larger heterogeneities in the coacervate are larger than was probed by the SAXS measurement, so we cannot comment on any effect of the SDS on the size of these. The high outlier in *n* at 1.5 mM (Figure 6a) is from the fit that included the additional term for the structure of the micelles, which may not have been necessary.

Figure 6b illustrates the chain correlation length from the fits. For network polymers, this ξ_L term is typically associated with the mesh size.[75, 76] At low $[SDS]_{sol}$, there is a clear correlation peak in the scattering that is attributed to the self-assembly of the Pluronic within the coacervate. These micelles act as large associating centers for the coacervates. As SDS is added, the effective mesh size decreases. The overall composition of the coacervates is essentially constant below 2 mM (Table 1), so these changes in the correlation length are associated with the distribution of polymer chains in the coacevate. With the addition of SDS, the micelle size decreases, so the density of micelles that can associate with the PAA increases as the Pluronic concentration remains invariant. This is essentially analogous to increasing the crosslinker density in hydrogels, which leads to smaller mesh sizes. At $[SDS]_{sol}$ =1.5 mM, the correlation peak associated with the micelles is not clear in the scattering data and these scattering data can be fit with either eqn (2) or eqn (3). The sizes associated with the q_0 and ξ_L terms appear to be correlated from eqn (3), which leads to significant uncertainty in these parameters. The small ξ_L reported at $[SDS]_{sol}$ =1.5 mM is likely not physically meaningful. However, these scattering data can be well fit with eqn (2) as shown in Figure S7, which indicates an increase in the correlation length after disruption of the micelles. This suggests a looser network of associated PAA-Pluronic is formed when the micelles are inhibited by the SDS. As shown in Figure 6b as the SDS concentration increases, there is a consistent near linear decrease in ξ_L. The average mesh size appears to decrease in the coacervate even as the water content increases (Figure 3). This likely is associated with relative compositional change in the coacervate with less Pluronic present where the additional PAA is less associated (more free AA segments) to produce smaller average distances between segments, which results in a decreased ξ_L.

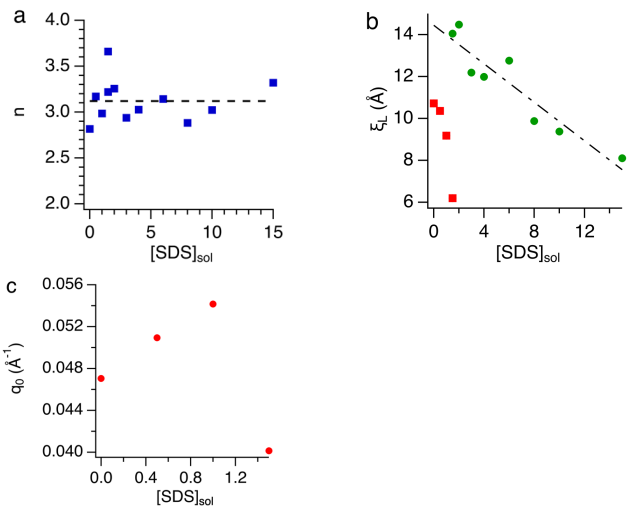

Fig. 6 Structural characteristics of the coacervates with different $[SDS]_{sol}$ determined from fits of the SAXS data in terms of **(a)** Porod exponent of the large electron density fluctuations where the dashed line is the average value (3.1), **(b)** chain correlation length in the coacervate, and **(c)** the momentum transfer vector (q) associated with the micelle size when the scattering could clearly demonstrate that micelles persisted in the coacervates. For the correlation length, the model choice impacts the best fit value with the data at $[SDS]_{sol}$ =1.5 mM well fit with both (●) eqn (2) and (■) eqn (3). The dashed lines provide a guide for the readers in terms of (a) average n and (b) linear decrease in ξ_L with increasing $[SDS]_{sol}$.

Figure 6c illustrates how the average size associated with the micelles change with $[SDS]_{sol}$. There is a general shift to higher *q* for the peak position as SDS is added until $[SDS]_{sol}$ = 1.5 mM. This corresponds to a decrease in the size, which is qualitatively consistent with prior investigations of Pluronic-SDS solutions[69]

and the DLS measurements shown in Figure 4. However, the coacervation appears to further disrupt the micellization of the Pluronic with no clear correlation peak observed in the scattering for $[SDS]_{sol} \geq 1.5$ mM in the coacervate, while the hydrodynamic radius appears to remain larger than the Pluronic unimer for higher SDS concentrations. As the phase transition to the coacervate is driven by the association between the EO and AA on the polymer chains, it is not surprising that there is some shift in the thermodynamics driving the micellization of the Pluronic. When there is not a clear peak in the scattering data ($[SDS]_{sol}$ = 1.5 mM), the fit length scales of q0 and ξ_L do not appear to be independent and results in a larger spacing (smaller q_0) as shown in Figure 6c and a smaller correlation length (ξ_L) as shown in Figure 6b. Fitting these same data with one less term in the model results in ξ_L that is consistent with the trend in higher $[SDS]_{sol}$ data when using the same model. The discontinuity in ξ_L is attributed to the mixed micelle to unimer transition within the coacervate.

3.3 Impact of SDS on the rheological properties of coacervates

These changes in the structure of the coacervates should be directly correlated with their viscoelastic properties, although these properties for coacervates are strongly dependent on a variety of factors.[83] To understand the viscoelastic properties, small amplitude oscillation shear (SAOS) was applied to the coacervates. These SAOS measurements demonstrate that SDS concentration modulates the rheological properties of the PAA/F108 coacervate (Figure S8). Figure 7 illustrates the frequency dependent rheological properties of the coacervates with different SDS content. In all cases, the storage and loss moduli increase with increasing frequency. Comparison of the storage and loss moduli (Figure 7a and 7b) indicate that the moduli decrease as the SDS concentration increases. In all cases, the loss modulus is larger than storage modulus, which indicates that PAA/F108 coacervate always behaves as a viscoelastic liquid. This liquid-like behavior indicates that the hydrogen bond associations that can form networks are relatively short lived in comparison to the frequencies examined. The SAOS data for all of the coacervate concentrations are shown in Figure S8.

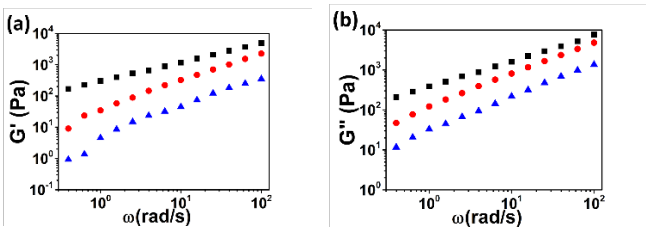

Fig. 7. Angular frequency (ω) dependence of the **(a)** storage modulus (G') and **(b)** loss modulus (G'') of coacervates prepared at $[SDS]_{sol}$ of (■) 0 mM, (●) 4 mM, and (▲) 15 mM.

These rheological data provide additional insights into the effect of SDS on the viscoelastic properties of these coacervates. As shown in Figure 8a, the addition of SDS decreases the storage modulus more than the loss modulus. The softening of these coacervates is consistent with the reported rheology of Pluronic F108 solutions and gels with the addition of SDS, but this prior study examined cases where the SDS concentration was much greater than its CMC.[77] The root cause of this decrease in the modulus was the disruption of the Pluronic packing by SDS with an isothermal transition from gel to liquid with addition of 10xCMC SDS.[77] The rheological data for the coacervates reported here also demonstrate a significant decrease in the storage modulus, which is consistent with the SDS disrupting the packing of the Pluronic to alter the physical network formed by the complexation of the PAA and Pluronic. Interestingly, there is nearly an order of magnitude decrease in G' between $[SDS]_{Sol}$ = 6 mM and 8 mM. There are no clear qualitative changes in the structure from the SAXS profiles (Figure S7) in the concentration range, but there is a large decrease in ξ_L from 12.8 Å at 6mM to 9.9 Å at 8 mM as shown in Figure 6b. This suggests that the effective mesh size of the coacervate is an important factor in its rheological response. At the highest SDS concentrations examined (10-20 mM), G' and G'' are nearly invariant, which is consistent with the similar SAXS patterns (Figure S7) at high $[SDS]_{Sol}$. However, the F108 concentration decreases by a factor of 3 (Table 1) over this range, which suggests that the coacervate formed under these conditions is behaving like a concentrated polymer solution as the loss of one associating polymer is not significantly altering the rheological properties.

To better illustrate the large change in rheological properties of the coacervate between $[SDS]_{Sol}$ = 6 mM and 8 mM, Figure 8b illustrates the loss factor determined from the SAOS measurements at 1 rad/s. The coacervates with $[SDS]_{Sol} \geq 8$ mM exhibit a much larger tan δ. This behavior is also consistent with the coacervates at high $[SDS]_{Sol}$ appearing more like solutions. Figure 8b suggests that there is a change in the connectivity or strength of the physical network of the coacervate near 8 mM SDS. Interestingly, this transition occurs very close to the known CMC of SDS.[73] This suggests that the inclusion of SDS micelles during the formation of the coacervate alters the physical network substantially to produce a much more fluid coacervate. It should be noted that there is not a dramatic change in the concentration of SDS within the coacervate (see Table 1 and Figure 2) in this range for $[SDS]_{Sol}$.

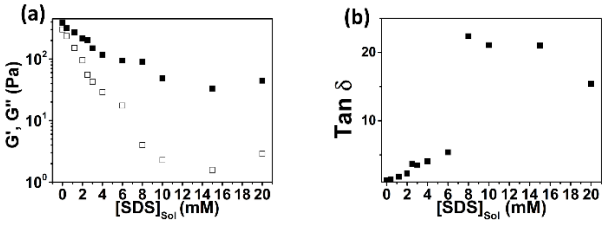

Fig. 8 Rheological properties of coacervates of PAA/F108/SDS at 1 rad/s as a function of $[SDS]_{Sol}$ in terms of **(a)** storage modulus (G', □), loss modulus (G", ■) and **(b)** tan δ.

Prior work examining the rheological properties of PECs has identified the water content as a key variable, where swelling-modulus master curves were obtained for a variety of complexes.[84] Figure 9 illustrates how the rheological properties of the PAA/F108/SDS coacervates depends on water content.

As might be expected based on prior work on PECs,[84] there is an approximately linear relationship between log moduli and water content in the coacervate between 52 and 60 wt % water. At higher water concentration, the moduli become essentially independent of water content. This invariant modulus occurs when $[SDS]_{Sol}$ is near the CMC of SDS and higher. This limited impact of water concentration over this narrow range is consistent with expectations for the moduli of concentrated polymer solutions.[85]

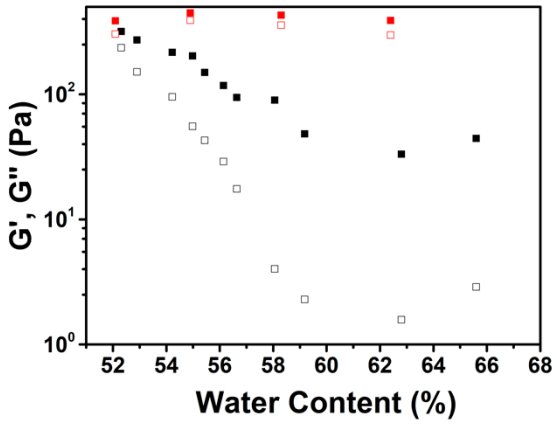

Fig. 9 Storage modulus (G', □) and loss modulus (G", ■) at 1 rad/s as a function of water content. The red symbol indicates the PAA/F108 coacervates formed without SDS at different pH to control the water content.

To further understand the influence of the SDS on the properties, the water content was varied in PAA/F108 coacervates without SDS by changing the pH between 2 and 3 as shown in Figure S9. These coacervates contain between 52 and 63 wt% water and no SDS. The SAXS data confirms that these coacervates all contain a well-defined micelle structure (Figure S10). The change in water content can be related to the ionization of the PAA at these different pH conditions.[46] As shown in Figure 9, the moduli of these coacervates prepared at different pH are nearly constant despite the change in water content. These results indicate that SDS disruption of the AA-EO associations is likely the origins of the changes in the rheological properties of these coacervates.

Additional work is necessary to determine the generality of these findings in terms of the surfactant examined and the nature of the polyelectrolyte pair in the coacervate. In particular, the order of combination of the components may be a critical factor as both the PAA and SDS interact with the Pluronic F108. In this case, the SDS was initially added to the Pluronic so some binding sites were likely occupied by SDS as the coacervate formed. This could produce a kinetically trapped structure in the coacervate. Initially mixing PAA and SDS would lead to a competitive adsorption scenario with the addition of Pluronic, while the SDS addition after formation of the PAA-Pluronic coacervate would likely be transport limited. However, prior work with a four component polyelectrolyte coacervate showed limited influence of addition order on the structure.[86]

4. Conclusions

The influence of a surfactant, SDS, on the structure and rheological properties of a coacervate of PAA and Pluronic F108 was systematically investigated. Without SDS, well defined micelles of F108 are present within the coacervate and the rheological properties of the coacervate are approaching a critical gel (G' = G'). Addition of SDS decreases the average size of the Pluronic micelles within the coacervate at low concentration with no features in the scattering associated with micelles resolved at $[SDS]_{Sol} \geq 1.5$ mM. The coacervate transitions from slightly F108 rich to strongly enriched with PAA as $[SDS]_{Sol}$ increases. This change is attributed with the association of SDS with the EO segments in the Pluronic to drive less efficient complexation between EO and AA. The storage and loss moduli of the coacervate both decrease with the addition of SDS, but storage modulus exhibits a larger decrease, which leads to an increase in the loss factor. There is a large increase in tan δ near the CMC of SDS (8 mM) with nearly an order of magnitude decrease in the storage modulus relative to the coacervate prepared at 6 mM. This change in property is accompanied by a decrease in the correlation length of the chains within the coacervate. We attribute this large change in the rheological properties to the loss of an effective physical network from the coacervation, such that the coacervates behave similar to concentrated polymer solutions. The storage modulus of these coacervates can be varied by 2 orders of magnitude with relatively low concentrations of SDS, while using pH to change the water content of PAA/F108 coacervates barely impacts the moduli.

Conflicts of interest

There are no conflicts to declare.

Acknowledgements

The authors acknowledge partial support from the National Science Foundation for this work through grant no. CMMI-1462284. Data reported here used the Complex Materials Scattering (CMS/11-BM) beamline, operated by the National Synchrotron Light Source II and the Center for Functional Nanomaterials, which are U.S. Department of Energy (DOE) Office of Science User Facilities operated for the DOE Office of Science by Brookhaven National Laboratory under Contract No. DE-SC0012704. The authors thank Masa Fukuto for his assistance with the x-ray measurements.

Notes and references

1. S. Huang, M. Zhao, M. B. Dawadi, Y. Cai, Y. Lapitsky, D. A. Modarelli and N. S. Zacharia, *J. Colloid Interface Sci.*, 2018, **518**, 216-224.
2. A. B. Marciel, S. Srivastava and M. V. Tirrell, *Soft Matter*, 2018, **14**, 2454-2464.

3. A. M. Rumyantsev, N. E. Jackson and J. J. de Pablo, *Ann. Rev. Condens. Mat. Phys., Vol 12, 2021*, 2021, **12**, 155-176.
4. Z. Y. Ou and M. Muthukumar, *J. Chem. Phys.*, 2006, **124**, 154902.
5. C. E. Sing, *Adv. Colloid Interface Sci.*, 2017, **239**, 2-16.
6. C. E. Sing and S. L. Perry, *Soft Matter*, 2020, **16**, 2885-2914.
7. A. F. Thunemann, M. Muller, H. Dautzenberg, J. F. O. Joanny and H. Lowen, *Polyelectrolytes with Defined Molecular Architecture II*, 2004, **166**, 113-171.
8. R. Chollakup, W. Smitthipong, C. D. Eisenbach and M. Tirrell, *Macromolecules*, 2010, **43**, 2518-2528.
9. R. Chollakup, J. B. Beck, K. Dirnberger, M. Tirrell and C. D. Eisenbach, *Macromolecules*, 2013, **46**, 2376-2390.
10. D. Priftis and M. Tirrell, *Soft Matter*, 2012, **8**, 9396-9405.
11. H. Dautzenberg, *Macromolecules*, 1997, **30**, 7810-7815.
12. Q. Wang and J. B. Schlenoff, *Macromolecules*, 2014, **47**, 3108-3116.
13. N. Volk, D. Vollmer, M. Schmidt, W. Oppermann and K. Huber, *Polyelectrolytes with Defined Molecular Architecture II*, 2004, **166**, 29-65.
14. B. Y. Yu, P. M. Rauscher, N. E. Jackson, A. M. Rumyantsev and J. J. de Pablo, *ACS Macro Lett.*, 2020, **9**, 1318-1324.
15. S. Gouin, *Trends Food Sci. Technol.*, 2004, **15**, 330-347.
16. R. A. Riggleman, R. Kumar and G. H. Fredrickson, *J. Chem. Phys.*, 2012, **136**, 024903.
17. F.-J. Ruiz, S. Rubio and D. Pérez-Bendito, *Anal. Chem.*, 2007, **79**, 7473-7484.
18. F. Fu and Q. Wang, *J. Environ. Manage.*, 2011, **92**, 407-418.
19. D. Eratte, B. Wang, K. Dowling, C. J. Barrow and B. P. Adhikari, *Food Funct.* 2014, **5**, 2743-2750.
20. S. M. D'Addio, C. Kafka, M. Akbulut, P. Beattie, W. Saad, M. Herrera, M. T. Kennedy and R. K. Prud'homme, *Mol. Pharmaceutics*, 2010, **7**, 557-564.
21. I. K. Voets, A. de Keizer and M. A. C. Stuart, *Adv. Colloid Interface Sci.*, 2009, **147-48**, 300-318.
22. S. Lindhoud, R. de Vries, W. Norde and M. A. C. Stuart, *Biomacromolecules*, 2007, **8**, 2219-2227.
23. A. Nolles, A. H. Westphal, J. A. de Hoop, R. G. Fokkink, J. M. Kleijn, W. J. H. van Berkel and J. W. Borst, *Biomacromolecules*, 2015, **16**, 1542-1549.
24. M. Danial, H. A. Klok, W. Norde and M. A. C. Stuart, *Langmuir*, 2007, **23**, 8003-8009.
25. S. Lindhoud, R. de Vries, R. Schweins, M. A. C. Stuart and W. Norde, *Soft Matter*, 2009, **5**, 242-250.
26. S. Srivastava, A. E. Levi, D. J. Goldfeld and M. V. Tirrell, *Macromolecules*, 2020, **53**, 5763-5774.
27. D. J. Audus, J. D. Gopez, D. V. Krogstad, N. A. Lynd, E. J. Kramer, C. J. Hawker and G. H. Fredrickson, *Soft Matter*, 2015, **11**, 1214-1225.
28. D. V. Krogstad, S.-H. Choi, N. A. Lynd, D. J. Audus, S. L. Perry, J. D. Gopez, C. J. Hawker, E. J. Kramer and M. V. Tirrell, *J. Phys. Chem. B*, 2014, **118**, 13011-13018.
29. J. H. Wang, S. T. Sun, B. H. Wu, L. Hou, P. Ding, X. H. Guo, M. A. C. Stuart and J. Y. Wang, *Macromolecules*, 2019, **52**, 8643-8650.
30. M. E. Seitz, W. R. Burghardt and K. R. Shull, *Macromolecules*, 2009, **42**, 9133-9140.
31. D. C. Tuncaboylu, A. Argun, M. Sahin, M. Sari and O. Okay, *Polymer*, 2012, **53**, 5513-5522.
32. C. Wang, C. G. Wiener, Y. M. Yang, R. A. Weiss and B. D. Vogt, *J. Polym. Sci. B, Polym. Phys.*, 2017, **55**, 1036-1044.
33. X. Wang, J. Lee, Y.-W. Wang and Q. Huang, *Biomacromolecules*, 2007, **8**, 992-997.
34. Y. Wang, K. Kimura, P. L. Dubin and W. Jaeger, *Macromolecules*, 2000, **33**, 3324-3331.
35. Q. Ru, Y. Wang, J. Lee, Y. Ding and Q. Huang, *Carbohydrate Polymers*, 2012, **88**, 838-846.
36. E. Spruijt, F. A. M. Leermakers, R. Fokkink, R. Schweins, A. A. van Well, M. A. C. Stuart and J. van der Gucht, *Macromolecules*, 2013, **46**, 4596-4605.
37. H. M. Fares, Y. E. Ghoussoub, J. D. Delgado, J. C. Fu, V. S. Urban and J. B. Schlenoff, *Macromolecules*, 2018, **51**, 4945-4955.
38. S. A. Kim, K. J. Jeong, A. Yethiraj and M. K. Mahanthappa, *Proc. Natl. Acad. Sci. USA*, 2017, **114**, 4072-4077.
39. H. Rehage and H. Hoffmann, *Mol. Phys.* 1991, **74**, 933-973.
40. O. Ikkala and G. ten Brinke, *Chem. Commun.*, 2004, 2131-2137.
41. P. Hansson and B. Lindman, *Curr. Opin. Colloid Interface Sci.*, 1996, **1**, 604-613.
42. A. F. Thunemann, *Prog. Polym. Sci.*, 2002, **27**, 1473-1572.
43. N. Khan and B. Brettmann, *Polymers*, 2019, **11**, https://doi.org/10.3390/polym11010051.
44. W. W. Zhao and Y. L. Wang, *Adv. Colloid Interface Sci.*, 2017, **239**, 199-212.
45. J. C. Brackman and J. Engberts, *J. Colloid Interface Sci.*, 1989, **132**, 250-255.
46. M. M. Zhao, S. A. Eghtesadi, M. B. Dawadi, C. Wang, S. Y. Huang, A. E. Seymore, B. D. Vogt, D. A. Modarelli, T. B. Liu and N. S. Zacharia, *Macromolecules*, 2017, **50**, 3819-3831.
47. E. Kizilay, S. Maccarrone, E. Foun, A. D. Dinsmore and P. L. Dubin, *J. Phys. Chem. B*, 2011, **115**, 7256-7263.
48. A. M. Barbosa, I. J. B. Santos, G. M. D. Ferreira, M. D. H. da Silva, A. Teixeira and L. H. M. da Silva, *J. Phys. Chem. B*, 2010, **114**, 11967-11974.
49. P. Bahadur, P. Dubin and Y. K. Rao, *Langmuir*, 1995, **11**, 1951-1955.
50. M. Simon, E. Schneck, L. Noirez, S. Rahn, I. Davidovich, Y. Talmon and M. Gradzielski, *Macromolecules*, 2020, **53**, 4055-4067.
51. R. G. Larson, Y. Liu and H. L. Li, *J. Rheology*, 2021, **65**, 77-102.
52. Y. L. Liu, H. H. Winter and S. L. Perry, *Adv. Colloid Interface Sci.*, 2017, **239**, 46-60.
53. C. Monteux, G. G. Fuller and V. Bergeron, *J. Phys. Chem. B*, 2004, **108**, 16473-16482.
54. K. Thuresson, S. Nilsson and B. Lindman, *Langmuir*, 1996, **12**, 530-537.
55. M. M. Zhao, C. Wang, H. W. Jiang, M. B. Dawadi, B. D. Vogt, D. A. Modarelli and N. S. Zacharia, *Soft Matter*, 2019, **15**, 3043-3054.
56. M. Gradzielski and I. Hoffmann, *Curr. Opin. Colloid Interface Sci.*, 2018, **35**, 124-141.
57. S. Laquerbe, A. Carvalho, M. Schmutz, A. Poirier, N. Baccile and G. Ben Messaoud, *J. Colloid Interface Sci.*, 2021, **600**, 23-36.
58. U. Gulyuz and O. Okay, *Macromol. Symp.* 2015, **358**, 232-238.
59. L. Chiappisi, S. D. Leach and M. Gradzielski, *Soft Matter*, 2017, **13**, 4988-4996.
60. M. Zhao, C. Wang, H. Jiang, M. B. Dawadi, B. D. Vogt, D. A. Modarelli and N. S. Zacharia, *Soft Matter*, 2019, **15**, 3043-3054.

61. C. Wang, C. G. Wiener, Z. Cheng, B. D. Vogt and R. A. Weiss, *Macromolecules*, 2016, **49**, 9228-9238.
62. Y. L. Wang, K. Kimura, P. L. Dubin and W. Jaeger, *Macromolecules*, 2000, **33**, 3324-3331.
63. A. Y. Xu, E. Kizilay, S. P. Madro, J. Z. Vadenais, K. W. McDonald and P. L. Dubin, *Soft Matter*, 2018, **14**, 2391-2399.
64. M. N. Wang and Y. L. Wang, *Soft Matter*, 2014, **10**, 7909-7919.
65. R. Ganguly, V. Aswal, P. Hassan, I. Gopalakrishnan and S. Kulshreshtha, *J. Phys. Chem. B*, 2006, **110**, 9843-9849.
66. P. R. Desai, N. J. Jain, R. K. Sharma and P. Bahadur, *Colloids Surf. A*, 2001, **178**, 57-69.
67. E. Hecht and H. Hoffmann, *Langmuir*, 1994, **10**, 86-91.
68. E. Hecht, K. Mortensen, M. Gradzielski and H. Hoffmann, *J. Phys. Chem.*, 1995, **99**, 4866-4874.
69. S. Kancharla, N. A. Zoyhofski, L. Bufalini, B. F. Chatelais and P. Alexandridis, *Polymers*, 2020, **12**.
70. Y. Li, R. Xu, S. Couderc, D. M. Bloor, E. Wyn-Jones and J. F. Holzwarth, *Langmuir*, 2001, **17**, 183-188.
71. Y. Li, R. Xu, D. M. Bloor, J. F. Holzwarth and E. Wyn-Jones, *Langmuir*, 2000, **16**, 10515-10520.
72. Y. J. Nikas and D. Blankschtein, *Langmuir*, 1994, **10**, 3512-3528.
73. P. Mukerjee and K. J. Mysels, *Critical micelle concentrations of aqueous surfactant systems*, National Standard reference data system, 1971.
74. B. Hammouda, D. L. Ho and S. Kline, *Macromolecules*, 2004, **37**, 6932-6937.
75. T. Matsunaga, T. Sakai, Y. Akagi, U. I. Chung and M. Shibayama, *Macromolecules*, 2009, **42**, 6245-6252.
76. A. Lerch, F. Kafer, S. Prevost, S. Agarwal and M. Karg, *Macromolecules*, 2021, **54**, 7632-7641.
77. J. Nambam and J. Philip, *J. Phys. Chem. B*, 2012, **116**, 1499-1507.
78. M. Radhakrishna, K. Basu, Y. L. Liu, R. Shamsi, S. L. Perry and C. E. Sing, *Macromolecules*, 2017, **50**, 3030-3037.
79. F. J. Morin, M. L. Puppo and J. E. Laaser, *Soft Matter*, 2021, **17**, 1223-1231.
80. X. L. Zhang, J. Penfold, R. K. Thomas, I. M. Tucker, J. T. Petkov, J. Bent, A. Cox and R. A. Campbell, *Langmuir*, 2011, **27**, 11316-11323.
81. P. Alexandridis and T. A. Hatton, *Colloids Surf. A*, 1995, **96**, 1-46.
82. G. Gyulai, A. Magyar, J. Rohonczy, J. Orosz, M. Yamasaki, S. Bosze and E. Kiss, *Express Polym.Lett.*, 2016, **10**, 216-226.
83. E. Spruijt, M. A. C. Stuart and J. van der Gucht, *Macromolecules*, 2013, **46**, 1633-1641.
84. K. Sadman, Q. F. Wang, Y. Y. Chen, B. Keshavarz, Z. Jiang and K. R. Shull, *Macromolecules*, 2017, **50**, 9417-9426.
85. Y. Heo and R. G. Larson, *Macromolecules*, 2008, **41**, 8903-8915.
86. G. A. Mountain and C. D. Keating, *Biomacromolecules*, 2020, **21**, 630-640.